ELSEVIER

Journal of Alloys and Compounds 275–277 (1998) 651–656

Journal of ALLOYS AND COMPOUNDS

Yb_2BaCoO_5 magnetic and crystal structure determination from neutron scattering

J. Hernández-Velasco[a,*], R. Sáez-Puche[a], J. Rodríguez-Carvajal[b]

[a]*Dpto. Química Inorgánica, Fac. CC. Químicas, Universidad Complutense, E-28040 Madrid, Spain*
[b]*Lab. Léon Brillouin, CEA-CNRS, CE-Saclay, F-91191 Gif sur Yvette, Cedex, France*

Abstract

The magnetic and crystal structure of Yb_2BaCoO_5 have been studied from powder neutron diffraction. The compound crystallizes in the orthorhombic space group *Pnma*, with lattice parameters: $a=12.1745(2)$ Å, $b=5.6594(1)$ Å, $c=6.9993(1)$ Å. Bulk magnetic measurements reveal a jump in the temperature dependence of the susceptibility around 10 K, which corresponds to the antiferromagnetic ordering of the Yb^{3+} and Co^{2+} sublattices which is fully confirmed with neutron diffraction data. From the later, a magnetic structure with an identical cell to the chemical one ($\mathbf{k}=0$) has been proposed to explain the onset of new reflections due to magnetic scattering that develop below $T_N \approx 9.4$ K. The spin arrangement is described on the basis of C_xA_z symmetry modes for all magnetic sublattices. © 1998 Elsevier Science S.A.

Keywords: Antiferromagnetism; Neutron diffraction; Magnetic structure

1. Introduction

R_2BaCoO_5 oxides (R=rare earth) crystallize into two different structures depending on the R^{3+} size [1–5]. The existence of polymorphism has been observed in this system [6–8]. Both forms are orthorhombic and correspond to the *Immm* and *Pnma* space groups. Yb_2BaCoO_5 belongs to the later structural type [3,4], which is characterized by the seven-coordination of R^{3+}, while the Co^{2+} cations are located in isolated distorted square pyramids (CoO_5).

Antiferromagnetic (AF) behaviour has been shown by bulk magnetic measurements in both the *Immm* and *Pnma* R_2BaCoO_5 oxides [4,5]. A more detailed analysis of the neutron diffraction data, concerning the complex spin arrangements exhibited by most of these compounds, is now in progress [9,10]. Among them, Yb_2BaCoO_5 presents by far the simplest magnetic symmetry and is therefore the main subject of this paper.

2. Experimental details

The powder sample of Yb_2BaCoO_5 was prepared by solid state reaction from stoichiometric amounts of the high purity reactants: Yb_2O_3 (99.99%), $CoCO_3 \cdot nH_2O$ (99.999%) and $BaCO_3$ (A.R. grade). The mixture was ground and then heated under Ar flow in various steps of 24 h of firing with interruptions for regrinding and increasing the temperature from 1000° to 1350°C.

For the magnetic measurements a SQUID magnetometer MPMS-XL Quantum Design was used.

The neutron diffraction data for magnetic structure determination were obtained in the two axis diffractometer Pyrrhias located in the cold neutron guide G4 at the Orphée reactor of the Laboratoire Léon Brillouin, CEA-Saclay (France). The G 4-1 diffractometer is equipped with a pyrolitic graphite monochromator and a linear multidetector composed of 800 cells (BF_3) separated by 0.1° covering an angular range of 80° (2θ). The incident wavelength was $\lambda=2.426$ Å. A He cryostat was used in the temperature range RT to 1.5 K.

For the crystallographic characterization at RT, the high resolution powder diffractometer G 4-2 was used. This is a two axis diffractometer with a high take-off angle,

*Corresponding author. Tel.: 34 1 3944353; fax: 34 1 3944352; e-mail: golfogti@eucmax.sim.ucm.es

PII: S0925-8388(98)00412-5

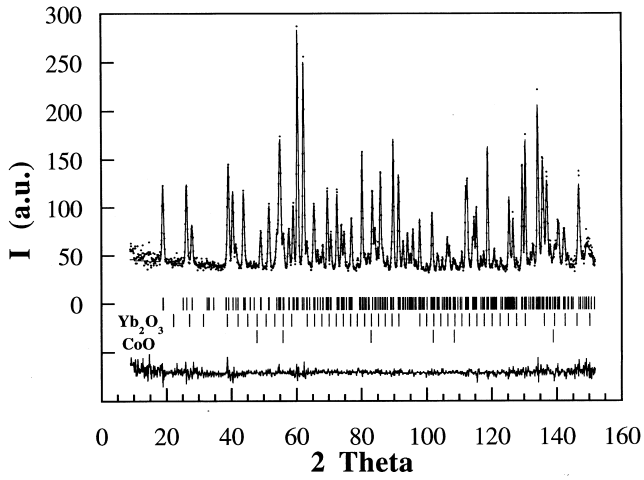

Fig. 1. Neutron diffraction pattern of Yb_2BaCoO_5 at RT. Experimental (dots), calculated (solid line) and difference at the bottom. Bragg reflections are marked by vertical lines.

equipped with a Ge monochromator which selecting the (115) reflection provides a wavelength $\lambda=1.9975$ Å. There is a bank of 10 ^{3}He detectors that measures the diffraction pattern by step scanning. The merged pattern covers an angular range of $2\theta<158°$.

The data were analyzed with the Rietveld method using the program Fullprof [11].

3. Results and discussion

3.1. Structural characterization

The neutron powder diffraction pattern at RT is shown in Fig. 1. The data have been fitted in the *Pnma* space group and the obtained lattice parameters are: $a=$ 12.1745(2) Å, $b=5.6594(1)$ Å, $c=6.9993(1)$ Å. Small amounts of parasitic phases Yb_2O_3 and CoO were detected and included in the Rietveld refinement. The obtained results are given in Table 1 and they agree with those previously reported from single crystal X-ray diffraction [3], but better accuracy is obtained for the light oxygen atoms. The structural features of *Pnma*-R_2BaCoO_5 oxides can be found elsewhere [4].

Table 1
Positions of atoms in the asymmetric unit of Yb_2BaCoO_5 at RT[a]

Atom	Site	x	y	z	B
Yb(1)	4*c*	0.2912(2)	$\frac{1}{4}$	0.1203(4)	0.61(5)
Yb(2)	4*c*	0.0740(2)	$\frac{1}{4}$	0.3994(3)	0.55(5)
Co	4*c*	0.6545(9)	$\frac{1}{4}$	0.6934(11)	0.49(24)
Ba	4*c*	0.9016(4)	$\frac{1}{4}$	0.9256(8)	0.74(12)
O(1)	8*d*	0.4347(3)	−0.0037(7)	0.1669(4)	0.78(8)
O(2)	8*d*	0.2255(3)	0.4976(7)	0.3620(5)	0.76(9)
O(3)	4*c*	0.1042(4)	$\frac{1}{4}$	0.0783(8)	0.89(11)
R_p	R_{wp}	R_{exp}	χ^2	R_f	R_B
11.0	9.62	7.93	1.47	2.48	3.40

[a] isotropic temperature factors (Å^2) and reliability factors (%).

3.2. Macroscopic magnetic behaviour

Magnetic susceptibility measurements in the temperature range from 1.7 to 400 K have been carried out and the results are plotted in Fig. 2. Above 50 K the data follows a Curie-Weiss law and the obtained effective magnetic moment for Yb^{3+} is $m=4.58\ \mu_B$, that agrees well with the calculated $g[J(J+1)]^{1/2}=4.54\ \mu_B$, after discounting the value for Co^{2+} $m=4.98\ \mu_B$, obtained from the isostructural compounds R_2BaCoO_5 (R=Lu and Y), where R^{3+} is a diamagnetic lanthanide [4].

Below 50 K deviations from linearity in the χ^{-1} vs T plot are observed due to the crystal field effect really marked in Yb^{3+}. Around 10.3 K an anomaly is seen that could be attributed to the 3D-AF-order discussed below.

In Fig. 3 the magnetization dependence with applied magnetic field down to 50 kOe at different temperatures is shown. The two upturns in the magnetization curves, which are better seen in the derivatives (See inset of Fig. 3), could correspond to two metamagnetic-like transitions. At 1.7 K they are observed around $H\approx2$ kOe and 46 kOe and, as expected, vanish above the ordering temperature $T_N\approx10$ K. Presumably these magnetic field induced transitions are due to the canting of ordered moments corresponding to the different magnetic atoms. Nevertheless the mechanism of this canting has to be better explored at higher fields, as saturation is not reached at 50 kOe, and preferably by anisotropic measurements in a single crystal of Yb_2BaCoO_5. However the determination of the magnetic structure at zero field must be first established.

3.3. Group theory analysis and magnetic structure characterization.

The experimental neutron diffraction data obtained at low temperatures reveal the onset of new peaks at $T_N\approx9.4$ K. Also there is a contribution to the intensity of the reflections in nuclear positions as can be seen in the first peak that appears at $2\theta\approx23.0°$ corresponding to the (200)+(101) reflections for which around half the intensity is due to magnetic scattering at 1.4 K, Fig. 4.

All the observed Bragg reflections can be indexed with a propagation vector $\mathbf{k}=0$. This means no loss in translational symmetry coming from the spin arrangement and so the magnetic cell dimensions are those of the chemical cell $a\times b\times c$. In this case the propagation vector group G_k has the whole symmetry of the point group *mmm* (D_{2h}), which contains the rotational parts of the crystallographic space group *Pnma*.

The three sets of magnetic atoms: Co, Yb(1) and Yb(2); are located in the 4*c* sites of *Pnma*, there are four Bravais

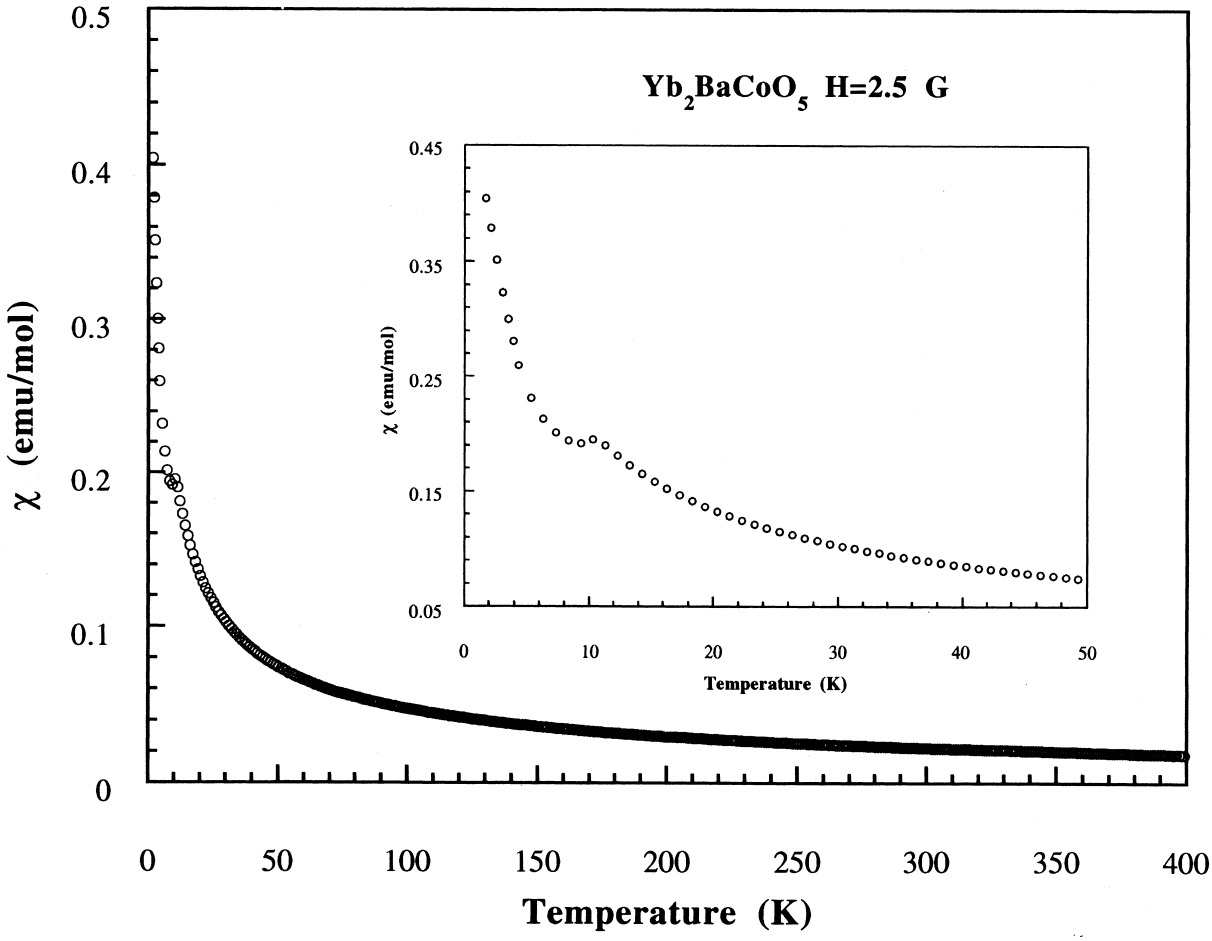

Fig. 2. Temperature dependence of the molar magnetic susceptibility. The inset shows the low temperature range.

sublattices numbered: 1 (x, $\frac{1}{4}$, z), 2 ($1/2-x$, $\frac{3}{4}$, $z+1/2$), 3 ($-x$, $\frac{3}{4}$, $-z$), 4 ($x+1/2$, $\frac{1}{4}$, $1/2-z$) and so there are 12 magnetic sublattices. We can build the eight 12-dimensional transformation matrices of the spin vectors under the symmetry operations of the group *mmm*, and with the characters of the irreducible representations (IR), given in Table 2, it is possible to generate the reducible representation $\Gamma = A_{1g} \oplus 2B_{2g} \oplus 2B_{3g} \oplus B_{4g} \oplus 2A_{1u} \oplus B_{2u} \oplus B_{3u} \oplus 2B_{4u}$ for the magnetic sublattices.

Following Bertaut [12–14], one defines the following basis vectors as linear combinations of the spin components: $F_\alpha = S_{1\alpha} + S_{2\alpha} + S_{3\alpha} + S_{4\alpha}$; $G_\alpha = S_{1\alpha} - S_{2\alpha} + S_{3\alpha} - S_{4\alpha}$; $C_\alpha = S_{1\alpha} + S_{2\alpha} - S_{3\alpha} - S_{4\alpha}$; $A_\alpha = S_{1\alpha} - S_{2\alpha} - S_{3\alpha} + S_{4\alpha}$; $\alpha = (x, y, z)$.

Using the spin transformation properties and the characters of the IR of the group is possible to obtain the components of the basis vectors of each IR by applying standard projection operators. Also it is possible to choose as generators of the *mmm* group the operations 2_x, 2_z and the inversion center i and apply them to the basis functions defined above. In both ways we obtain the possible magnetic modes, compatible with the crystallographic symmetry, describing the spin arrangement. These modes are summarized in the last columns of Table 2.

Although there are no general extinction rules it is worth noting some considerations about the intensity of the magnetic reflections, which is proportional to the square of the perpendicular component of the magnetic structure factor F_M to the scattering vector **Q**. We can write the former as following $F_M(\mathbf{Q}) \propto \Sigma \mathbf{m}_{kj} \exp[2\pi i(\boldsymbol{\tau} + \mathbf{k})\mathbf{r}_j]$ where $\mathbf{m}_{kj}$ is the vectorial Fourier component of the magnetic moment located at atom j in the position $\mathbf{r}_j$, and $\boldsymbol{\tau} = (h, k, l)$. In this case the reduced wave vector is $\mathbf{k} = (0,0,0)$, which taking into account the atomic positions in the Wyckoff site 4*c* yields $F_M = 0$ for a reflection of the type $(0, k, 0)$ when the coupling between spin components corresponds to a *G* or *C* mode. So the high intensity reflection that appears at $2\theta \approx 24.8°$ indexed as (010), which is forbidden in the crystal space group *Pnma*, is a purely magnetic one that is only allowed for *F* or *A* modes. Thus we can leave out the Γ_1 and Γ_7 representations describing magnetic structures on the basis of pure *G* and *C* modes respectively. Moreover, the representation Γ_4 can also be disregarded considering than a pure F basis vector describes a ferromagnetic order along the **b**-axis which is not the observed behaviour from bulk magnetic measurements as shown above, Fig. 2. In the same way Γ_2 and Γ_3 can be ignored, since they also involve a ferromagnetic

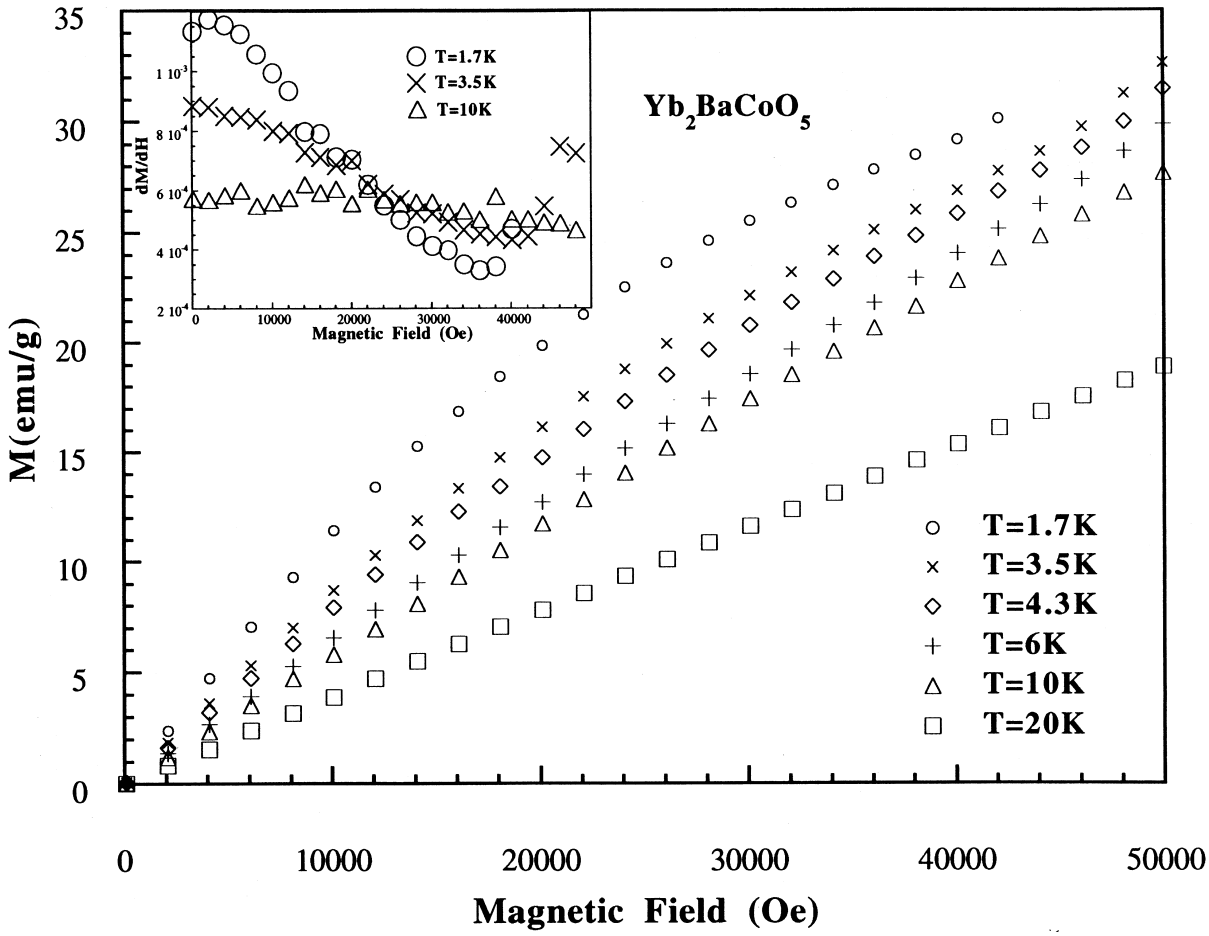

Fig. 3. Magnetization isotherms at the indicated temperatures versus applied magnetic field. The derivatives are shown in the inset.

component mixed with a *G* mode. Furthermore the Γ_6 (A_y) representation does not seem to agree with a strong reflection (010) because of the reason mentioned earlier

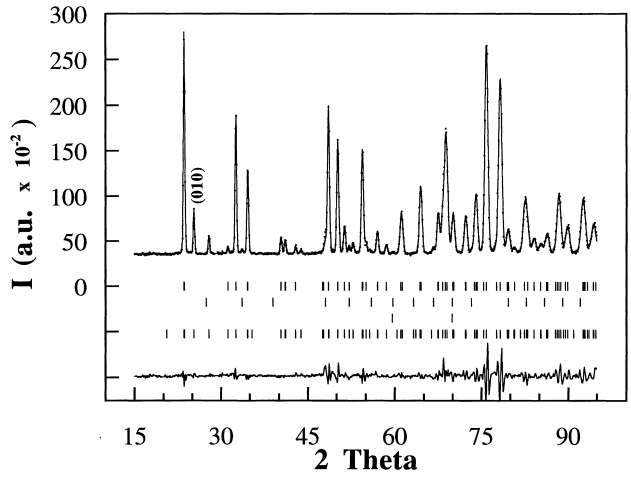

Fig. 4. Neutron diffraction pattern at 1.4 K fitted by taking into account the model for the magnetic order described in text. Last row of vertical marks indicates the allowed magnetic reflections. Discrepancy factors: $\chi^2=9.5$, $R_M=3.5\%$.

$I(hkl)\propto[F_M\perp(Q)]^2$, this peak must show contribution of the scattering due to spins along the *x* or *z* directions.

Finally, the fitting of the experimental data, Fig. 4, fully agrees with all the magnetic sublattices coupled within the same IR Γ_8 (C_xA_z). It corresponds, in the framework of magnetic space groups, to the Shubnikov symbol *Pnm'a*, where the elements associated with time reversal are just those chosen as generators. This can be easily inferred from the characters of the eight one-dimensional representations given in Table 2. Thus, the magnetic moments lie within the **ac** plane, as shown in Fig. 5.

From the analysis of the neutron diffraction patterns at different temperatures we can conclude that rare earth and Co^{2+} sublattices order at the same critical temperature $T_N\approx9.4$ K, but the evolution of the magnetic moments is quite different, see Table 3 and Fig. 6. The $\mathbf{m}_{Co}$ increases rapidly when temperature decreases and the saturation value is 4.1(1) μ_B, higher than $2\mathbf{S}=3\mu_B$ due to the strong orbital contribution **L**. The ordered $\mathbf{m}_{Yb(2)}$ slightly goes up from 1.2(2) μ_B at 9.4 K, but is near its saturation value of 1.61(9) μ_B in the whole temperature range, while $\mathbf{m}_{Yb(1)}$ is very small above 1.4 K, around 0.4–0.3 μ_B, retaining a degree of disorder till the lowest temperature, where it increases up to 1.07(8) μ_B. This could explain the suscep-

Table 2
Character table of irreducible representations for *Pnma* (**k**=0), basis vector components and magnetic space groups

mmm	1	2_x	2_y	2_z	*i*	m_x	m_y	m_z	*x*	*y*	*z*	G_M
Γ_1 (+++) A_{1g}	1	1	1	1	1	1	1	1		*G*		*Pnma*
Γ_2 (−++) B_{2g}	1	−1	−1	1	1	−1	−1	1	*G*		*F*	*Pn'm'a*
Γ_3 (+−+) B_{3g}	1	1	−1	−1	1	1	−1	−1	*F*		*G*	*Pnm'a'*
Γ_4 (−−+) B_{4g}	1	−1	1	−1	1	−1	1	−1		*F*		*Pn'ma'*
Γ_5 (++−) A_{1u}	1	1	1	1	−1	−1	−1	−1	*A*		*C*	*Pn'm'a'*
Γ_6 (−+−) B_{2u}	1	−1	−1	1	−1	1	1	−1		*A*		*Pnma'*
Γ_7 (+−−) B_{3u}	1	1	−1	−1	−1	−1	1	1		*C*		*Pn'ma*
Γ_8 (−−−) B_{4u}	1	−1	1	−1	−1	1	−1	1	*C*		*A*	*Pnm'a*

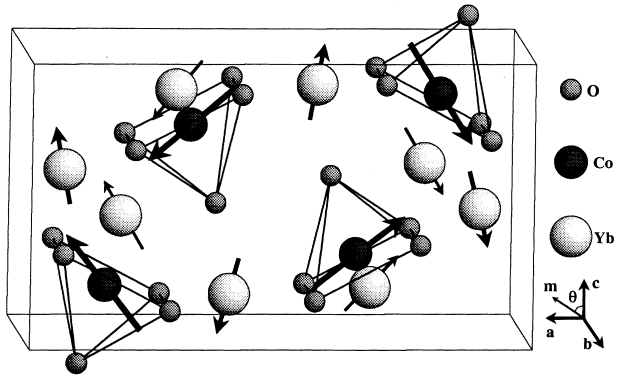

Fig. 5. Representation of the magnetic structure of Yb_2BaCoO_5 at 1.4 K. The only diamagnetic atoms plotted are those showing the Co coordination.

Table 3
Magnetic moments (μ_B) for Yb^{3+} and Co^{2+} in Yb_2BaCoO_5 at 1.4 K in cartesian and spherical coordinates[a]

	Co	Yb(1)	Yb(2)
m_x	3.04(11)	−0.64(9)	−0.43(8)
m_y	0	0	0
m_z	−2.72(9)	0.86(6)	−1.55(9)
m	4.08(12)	1.07(8)	1.61(9)
θ	132°(1)	−37°(4)	195°(2)

[a] θ angle defined in Fig. 5.

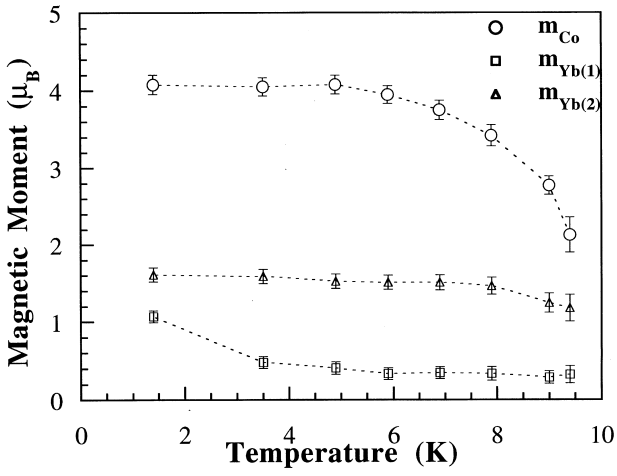

Fig. 6. Thermal evolution of the ordered magnetic moments in Yb_2BaCoO_5 below the Néel temperature. Dashed lines are guides.

tibility behaviour, Fig. 2, where the increasing signal when lowering temperature below T_N may be due to the almost paramagnetic state of Yb(1). The values of both $\mathbf{m}_{Yb}$ are low compared with the theoretical non-interacting moment $\mathbf{gJ}=4\mu_B$, this is due to the splitting of the ground multiplet by the crystal field in this Kramers ion ($^2F_{7/2}$) with a breaking of degeneracy, furthermore Yb^{3+} is the smallest magnetic rare earth cation and because of the lower interatomic distances the effect of the crystal field is drastically increased. So this substantial difference between theoretical and experimental $\mathbf{m}_{Yb}$ values is in the usual relationship found in Yb magnetically ordered compounds. For example in related oxides such as $Yb_2Cu_2O_5$, the value of $\mathbf{m}_{Yb}=1.4\ \mu_B$ has been reported [15]. In the isostructural compound Yb_2BaCuO_5 very weak magnetic reflections indexed with a propagation vector $\mathbf{k}=[0, \frac{1}{2}, \frac{1}{2}]$ have been invoked at 1.3 K but the magnetic structure remains unsolved [16]. In *Pnma*-Yb_2BaNiO_5 no order has been observed down to 1.4 K [17]. So the magnetic order of the Co spins has marked importance in polarizing the rare earth sublattices.

With respect to the remaining *Pnma*-R_2BaCoO_5, very different magnetic spin arrangements have been found, which occur with an underlying loss of translational symmetry respect to the paramagnetic space group ($\mathbf{k}\neq 0$) including various complex phase transitions [9]. The reason for this is the marked differences on the specific electronic configuration of R^{3+} where the anisotropic forces play an important role.

Acknowledgements

We thank the Spanish CICYT (Project MAT95-0809) and J. Hernández-Velasco also wishes to thank the ERES committee for a financial support grant.

References

[1] H. Mevs, Hk. Müller-Buschbaum, J. Less-Common Met. 152 (1989) 139.
[2] H. Mevs, Hk. Müller-Buschbaum, Z. Anorg. Allg. Chem. 573 (1989) 128.

[3] H. Mevs, Hk. Müller-Buschbaum, Z. Anorg. Allg. Chem. 574 (1989) 172.
[4] J. Hernández-Velasco, A. Salinas-Sánchez, F. Fernández, R. Sáez-Puche, J. Alloys Comp. 203 (1994) 15.
[5] J. Hernández-Velasco, A. Salinas-Sánchez, R. Sáez-Puche, J. Solid State Chem. 110 (1994) 321.
[6] J. Hernández-Velasco, R. Sáez-Puche, J. Alloys Comp. 198 (1993) 63.
[7] J. Hernández-Velasco, R. Sáez-Puche, J. Alloys Comp. 225 (1995) 147.
[8] E. Kluver, Hk. Müller-Buschbaum, Z. Anorg. Allg. Chem. 619 (1993) 421.
[9] J. Hernández-Velasco, Ph. D. Thesis. Universidad Complutense de Madrid, 1998.
[10] J. Hernández-Velasco, R. Sáez-Puche, J. Rodríguez-Carvajal, Physica B. 234–236 (1997) 569.
[11] J. Rodríguez-Carvajal, Physica B 192 (1993) 55.
[12] E.F. Bertaut, in: G.T. Rado, H. Suhl, Magnetism, Vol. III, ch. 4, Academic Press, New York 1963, p. 149.
[13] E.F. Bertaut, Acta Crystallogr. A. 24 (1968) 217.
[14] E.F. Bertaut, J. Phys (Paris), Coll. C1 (Suppl. 2–3)., 32 (1971) 1–462.
[15] J.L. García-Muñoz, J. Rodríguez-Carvajal, M. Vallet-Regí, J. González-Calbet, M. Parras, Phys. Rev. B. 44(9) (1991) 4716.
[16] I.V. Golosovskii, V.P. Plakhtii, V.P. Kharchenkov, J. Zoubkova, B.V. Mill, M. Bonnet, E. Roudaut, Sov. Phys. Solid State 34(5) (1992) 782.
[17] E. García-Matres, Ph. D. Thesis. Universidad Autónoma de Madrid, 1994.